Experimental Demonstration of Enhanced Self-Amplified Spontaneous Emission by an Optical Klystron

G. Penco,[1,*] E. Allaria,[1] G. De Ninno,[1,2] E. Ferrari,[1,3] and L. Giannessi[1,4]

[1]*Elettra-Sincrotrone Trieste S.C.p.A., Strada Statale 14 - km 163.5 in AREA Science Park, 34149 Basovizza, Trieste, Italy*

[2]*Laboratory of Quantum Optics, University of Nova Gorica, 5001 Nova Gorica, Slovenia*

[3]*Università degli Studi di Trieste, Dipartimento di Fisica, Piazzale Europa 1, 34100 Trieste, Italy*

[4]*Enea, via Enrico Fermi 45, 00044 Frascati, Roma, Italy*

(Received 22 October 2014; published 6 January 2015)

We report the first experimental evidence of enhancement of self-amplified spontaneous emission, due to the use of an optical klystron. In this free-electron laser scheme, a relativistic electron beam passes through two undulators, separated by a dispersive section. The latter converts the electron-beam energy modulation produced in the first undulator in density modulation, thus enhancing the free-electron laser gain. The experiment has been carried out at the FERMI facility in Trieste. Powerful radiation has been produced in the extreme ultraviolet range, with an intensity a few orders of magnitude larger than in pure self-amplified spontaneous emission mode. Data have been benchmarked with an existing theoretical model.

DOI: 10.1103/PhysRevLett.114.013901 PACS numbers: 42.65.Re, 41.50.+h, 41.60.Cr

Since the discovery of lasers [1,2], continuous progress in the development of coherent sources has provided invaluable investigation tools to the scientific community. In this framework, free-electron lasers (FELs) are now playing an important role with the construction and operation of large infrastructures, offering the possibility to extend many of the investigation techniques previously implemented with optical lasers to the vacuum ultraviolet (VUV), soft x-ray [3–5], and hard x-ray [6,7] wavelengths.

The first FELs were based on the oscillator configuration [8] where an ultrarelativistic electron beam passing through an undulator magnet interacts with the emitted radiation stored in an optical cavity. Oscillator FELs were realized in an extremely wide spectral range, from the THz [9,10] to the VUV [11–18]. Progress in the technology of FEL oscillators was provided by the optical klystron configuration [19,20]. The optical klystron consists of two undulators separated by a dispersive section, an element converting the beam-energy modulation induced by the first undulator into a longitudinal density modulation which enhances the emission in the second undulator. This process, which naturally occurs in a sufficiently long undulator, can be controlled in an optical klystron by fine-tuning the value of the dispersion. This parameter can be optimized to simultaneously maximize the FEL efficiency while minimizing the signal rise time to reach saturation.

The optical klystron configuration was adopted in most FELs operating in the UV and VUV spectral range [11–18]. However, further decreasing the wavelength required a complete configuration change. The lack of mirrors that could provide sufficient reflectivity to sustain the lasing process in a oscillator cavity forced the design of FELs in single-pass high-gain configurations where the interaction takes place in a long sequence of undulators.

In the self-amplified spontaneous emission (SASE) configuration, this long FEL amplifier is seeded by the incoherent spontaneous radiation emitted by the beam in the first part of the undulator [21]. The laser power grows exponentially along the undulator with a folding length $L_g = \lambda_u/(4\pi\sqrt{3}\rho)$ [21–23], where ρ is a characteristic dimensionless parameter of the FEL [23,24], typically in the range from 10^{-4} to 10^{-3}, depending on the FEL properties and operation spectral range. Saturation is reached after about 20 L_g, a length which can be of the order of $\sim$100 m in hard x rays.

A possibility to reduce the overall saturation length in a SASE amplifier consists in implementing the optical klystron concept previously introduced in the frame of FEL oscillators. Theoretical studies [25–29] have shown that the increase in density modulation induced by the optical klystron dispersive section significantly reduces the total length of the undulator needed to reach saturation.

In this Letter, we present the first experimental demonstration of the optical klystron output power enhancement in a SASE FEL in the VUV regime. The experiment has been performed at the FERMI facility [4]. The layout of the FEL is shown in Fig. 1. Even if the first undulator before the dispersive section and the other undulators in the long final amplifier have different periods, this configuration is perfectly suited to test the high-gain optical klystron scheme by adjusting the undulator gaps and tuning the resonance of all undulators at the same resonant wavelength.

The optical klystron performance in a high-gain FEL is strongly influenced by the electron beam relative uncorrelated energy spread δ, which has to be much smaller than the FEL parameter ρ. We report here the 1D approximate

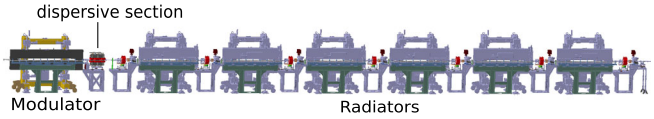

FIG. 1 (color online). FERMI FEL sketch including the 3-m-long modulator (planar undulator with a period of 100.3 mm), the dispersive section (three-pole wiggler with an overall length of 700 mm) and six 2.3 m long radiators (Apple II undulator, with a period of 55.2 mm and tunable both in linear and in circular polarization).

expression of the optical klystron power gain G relative to the value in pure SASE mode, as obtained in [29]:

$$G \approx \frac{1}{9}[5 + D^2 e^{-(D^2\delta^2/\rho^2)} + 2\sqrt{3}De^{-(D^2\delta^2/2\rho^2)}], \qquad (1)$$

where $\lambda_r = 2\pi/k_r$ is the resonant wavelength, $D = k_r R_{56}\rho$, and R_{56} is the momentum compaction of the dispersive section. It is straightforward to obtain from Eq. (1) the maximum theoretical power gain factor $G_{\max}$, that occurs when $R_{56}k_r\delta = 1$,

$$G_{\max} \approx \frac{1}{9}\left[5 + \left(\frac{\rho}{\delta}\right)^2 e^{-1} + 2\sqrt{3}\left(\frac{\rho}{\delta}\right)e^{-1/2}\right] \qquad (2)$$

Equation (2) confirms that the smaller uncorrelated energy spread the beam has, the higher $G_{\max}$ is expected to be.

In the experiment conducted at FERMI, the dispersive section has been exploited to enhance the bunching induced by the spontaneous emission produced in the modulator. The main parameters of the electron bunch are listed in Table I.

FERMI has been designed to operate in high-gain harmonic generation (HGHG) mode [30]. The electron bunch has therefore strong requirements concerning the slice energy spread, which has to be several times smaller than the ρ parameter [31]. The electron beam generated by the photoinjector [32] is compressed about 10 times by means of a magnetic chicane compressor [33] to obtain a bunch with a peak current of about 500 A. Microbunching instability, driven by coherent synchrotron radiation [34] occurring during the compression process and by longitudinal space charge forces along the linac [35], could degrade the final uncorrelated energy spread affecting the FEL performance. For this reason, a laser heater system [36] was installed after the photoinjector [37], at about 100 MeV, to properly increase the small natural uncorrelated energy spread from the photocathode rf gun and to suppress the microbunching instability growth. It has been demonstrated [38] that a fine-tuning of the laser heater intensity, around 0.5–1.0 μJ, permits us to constrain the relative uncorrelated energy spread after the compression and the linac transport to less than 10^{-4} (i.e., $\simeq\rho/20$ in the considered experimental conditions), with a relevant improvement in the FEL output performance [37].

TABLE I. Main parameters of the electron bunch.

Parameter	Value	Unit
Beam energy	1.05	GeV
Peak current	500	A
Slice normalized emittance	1.0	mm mrad
Bunch length (rms)	300	fs
Beam spot size at the radiator (rms)	100	μm

In our experiment, we tuned both modulator and radiator at 43 nm and without activating the dispersive section we produced a SASE FEL output of few microjoules. In particular, the radiator undulators are tuned in circular polarization to increase the FEL pulse energy. Then, we tuned the dispersive section R_{56} in the range 0 to 300 μm while measuring the progressive increment of the FEL pulse energy associated with the optical klystron enhancement. We have furthermore studied the behavior of the optical klystron at different laser heater intensities. Figure 2 shows some relevant cases.

The FEL output energy has been measured shot-to-shot by means of calibrated gas cells [39] and each point in the curves corresponds to the average over 20 consecutive shots; the error bar corresponds to the standard error of the measurement. We call R_{56}^{opt} the experimental value of R_{56} that maximizes the optical klystron FEL pulse energy. The case of the laser heater at 0.8 μJ (blue squares in Fig. 2) is very close to the laser-heater setting that minimizes the slice energy spread and the corresponding value of R_{56}^{opt} is 84 μm. Increasing the intensity of the laser heater induces larger slice energy spread that depletes the optical klystron FEL gain and shifts the R_{56}^{opt} towards lower values (see red triangles and green diamond points).

Table II reports the values of R_{56}^{opt} measured in the three cases plotted in Fig. 2 and the relative slice energy spread (δ) of the electron beam at the undulator as inferred

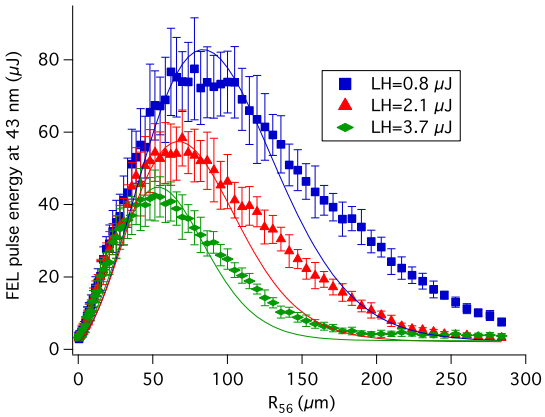

FIG. 2 (color online). FEL output energy in optical klystron SASE regime at 43 nm versus the chicane R_{56} for different laser-heater intensities. Solid lines correspond to the theoretical gain factor G calculated in each case by using Eq. (1).

TABLE II. Relative slice energy spread δ calculated from the condition $R_{56}^{\mathrm{opt}} k_r \delta = 1$ for different laser heater configurations when the optical klystron FEL is tuned at 43 nm.

LH energy (μJ)	δ	R_{56}^{opt} (μm)
0.8	8.1×10^{-5}	84 ± 5
2.1	1.0×10^{-4}	67 ± 4
3.7	1.3×10^{-4}	54 ± 3

by the condition $R_{56}^{\mathrm{opt}} k_r \delta = 1$. In all cases, δ results to be significantly smaller than the FEL ρ parameter, that is 1.7×10^{-3} in the described condition.

The optical klystron gain G vs R_{56} from Eq. (1) has been calculated in the three cases, by assuming $\rho = 1.7 \times 10^{-3}$ and the value of δ defined in Table II. The predicted optical klystron FEL energy per pulse has been obtained multiplying the SASE pulse energy measured at $R_{56} = 0$ by G. The results are plotted in Fig. 2 (solid lines) for comparison with the measurements.

The model behind Eq. (1) relies on the strong assumption that the beam energy distribution over a radiation wavelength is Gaussian and independent from the position along the bunch, with a second moment that we indicate as δ_{λ_r}. However, in a real electron beam, collective effects such as the microbunching instability, lead to a dependence of the energy distribution from the bunch longitudinal position. We can therefore define the energy spread δ_{FEL} as that one calculated over the longitudinal scale affecting the FEL gain, i.e., the FEL cooperation length $L_c = \lambda_r / 4\pi\rho$. The energy spread δ_{FEL} can be larger than δ_{λ_r}, leading to a reduced FEL emission.

In our measurements, when the laser-heater intensity is very low (blue square data in Fig. 2), and the microbunching instability is not completely suppressed, experimental data and model expectations agree only qualitatively. On the other side, when the laser heater is strong enough to almost suppress the microbunching instability (green diamond data), the increased energy spread δ_{λ_r} is comparable to δ_{FEL}, and the model is in agreement with the experiment results.

In order to maximize the optical klystron FEL pulse energy, it is necessary to find the best compromise between microbunching instability suppression and a small induced slice energy spread; thus a fine-tuning of the laser heater energy is required. For this purpose we have scanned the laser-heater intensity while keeping constant the R_{56} at 84 μm and the results are plotted in Fig. 3. Each data point is the statistical average over 20 consecutive shot-to-shot FEL pulses with an error bar corresponding to their standard error. The three laser-heater energy cases previously considered are reported on the same curve with the same markers used in Fig. 2.

We have exploited the optical klystron enhancement to the SASE process at other two wavelengths (32.4 nm and 20 nm), optimizing the laser-heater intensity to have the maximum FEL intensity. In order to better compare the three wavelengths explored, we have plotted in Fig. 4 the behavior of the measured optical klystron FEL intensity gain relative to the pure SASE (i.e., $R_{56} = 0$) as a function of the chicane R_{56}. We have calculated the theoretical $G_{\mathrm{max}}^{\mathrm{th}}$ by using Eq. (2) and assuming a slice energy spread which satisfies $R_{56}^{\mathrm{opt}} k_r \delta = 1$, and we listed the results in Table III. The obtained $G_{\mathrm{max}}^{\mathrm{th}}$ is in agreement (within 10%) with the peak of the gain factor measured in our experiment.

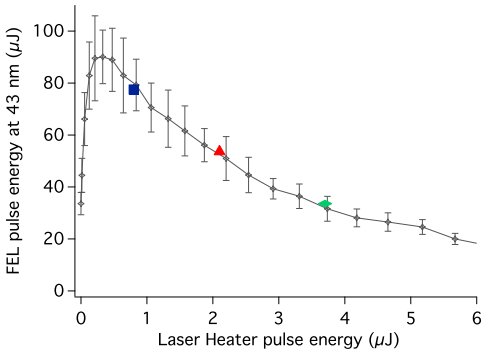

FIG. 3 (color online). FEL intensity at 43 nm in optical klystron configuration with $R_{56} = 84$ μm versus laser heater intensity. The three laser heater intensity cases (0.8 μJ, 2.1 μJ and 3.7 μJ) are plotted on the curve as blue, red, and green markers, respectively.

The low efficiency of the optical klystron at 20 nm is mainly due to the weak magnetic strength of the FERMI modulator at this wavelength [40]. In fact despite the large tuning range of the modulator, it has been designed to be resonant in the range from 200–300 nm, so that at 20 nm the poor coupling between the radiation and the electron beam translates to very small beam-energy modulation and consequently to small bunching.

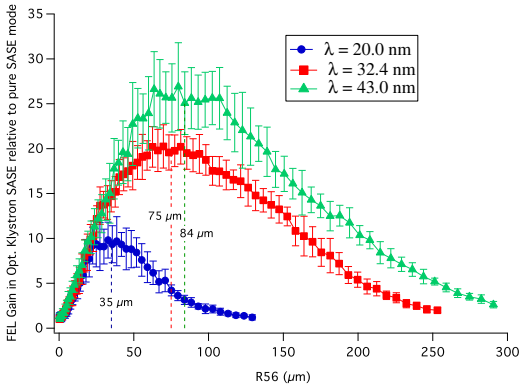

FIG. 4 (color online). SASE FEL relative enhancement through optical klystron at 43 nm, 32.4 nm and 20 nm. The optimum R_{56}^{opt} corresponding to the measured maximum gain is highlighted in the plot for each wavelength case. Each data point is the statistical average over 20 consecutive shot-to-shot FEL pulses with an error bar corresponding to their standard error.

TABLE III. The ρ parameter, the theoretical $G_{\max}^{\text{th}}$ as foreseen by Eq. (2), and the optimum R_{56}^{opt} for the FERMI optical klystron operating at 43 nm, 32.4 nm, and 20 nm.

λ_r (nm)	ρ	$\delta\ (=\delta_{\lambda_r})$	$G_{\max}^{\text{th}}$	R_{56}^{opt}
43	1.7×10^{-3}	8.1×10^{-5}	22.0	84 ± 5
32.4	1.3×10^{-3}	6.9×10^{-5}	19.8	75 ± 4
20	1.1×10^{-3}	9.1×10^{-5}	8.7	35 ± 2

The optical klystron scheme has been furthermore tested on the so-called FERMI FEL-2 line, consisting in a HGHG double-stage cascade, whose layout is well described in [5], which includes two dispersive sections. A fine-tuning of the latter allowed us to strongly enhance the pure SASE emission, obtaining intense photon pulses of about 100 μJ at 12 nm.

The optical klystron enhancement to the SASE process translates to a reduced number of undulators needed to reach the FEL saturation. In order to evaluate the actual advantage of this configuration, the FEL gain length has been calculated by measuring the exponential growth of the FEL output versus the number of resonant radiators (progressively detuning each radiator undulator).

The exponential gain of the optical klystron SASE at 32.4 nm for three values of R_{56} is reported in logarithmic scale in Fig. 5(a), and comparison with the corresponding gain curve of the seeded FEL operating in HGHG mode at the same wavelength is provided. In the latter case, the bunching is induced by an external seed. This allows obtaining significant emission already in the modulator (data at $z = 0$) and in the first radiator (data at $z = 2.34$ m). Instead, due to lethargy [41], the FEL provided by means of the optical klystron reaches a detectable level only after the second radiator but the exponential gain is more rapid, because of the smaller slice energy spread. The resulting gain length L_g is about 1.2 m, in very good agreement with the expected value provided by GENESIS 1.3 [42] simulations, and in addition it is very similar to the expected L_g in pure SASE mode. Increasing the R_{56} up to the optimum value leads to increasing the FEL emission after the second radiator but it does not affect the slope of the optical klystron SASE gain curve: the gain length is independent of the R_{56} setting and this is also confirmed by FEL simulations. At 32.4 nm, assuming a pure SASE saturation length of $\approx 20 L_g$, corresponding to an undulator length of 24 m, the optimization of the optical klystron [$R_{56} = 75$ μm (see Fig. 4)] would allow us to reach saturation saving about 15% of the total undulators length, with respect to standard SASE operation. Figure 5(b) shows three consecutive FEL spectra acquired in the optical klystron SASE configuration when all radiators are tuned at 32.4 nm. Averaging the spectrum profiles of 10 consecutive FEL pulses and fitting with a Gaussian curve provides an estimation of the optical klystron FEL spectrum bandwidth that turns out to be $\sigma_\lambda/\lambda = 3.3 \times 10^{-3} \sim 2\rho$.

In conclusion, the optical klystron enhancement to SASE FEL has been experimentally demonstrated at FERMI, providing extreme ultraviolet photons with energy per pulse on the order of 100 μJ. Our experiments have confirmed that the optical klystron FEL performance is strongly influenced by the electron beam relative uncorrelated energy spread, which must be significantly smaller than the FEL ρ parameter. The model in [29] can reproduce the experimental results when microbunching structures in the longitudinal phase space are fully

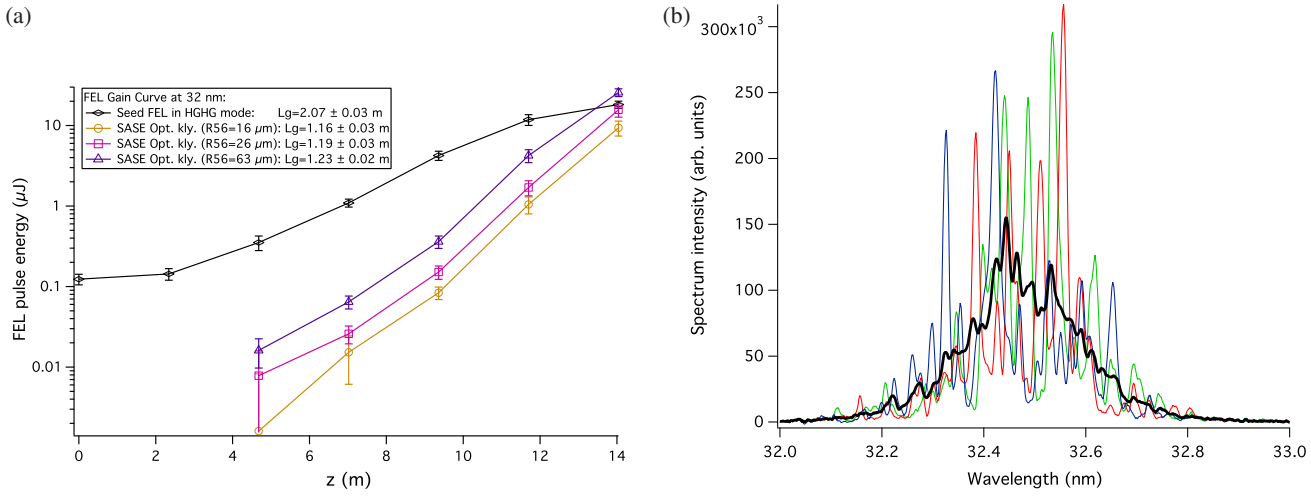

FIG. 5 (color online). (a) Comparison between the FEL gain curve measured in optical klystron SASE mode for different dispersive section settings and in HGHG seeded mode at 32.4 nm. Each data point corresponds to an undulator length (2.32 m). In the HGHG seeded FEL, we measured the output pulse energy also after the modulator and the first radiator. (b) Single-shot (color lines) optical klystron FEL spectra when all radiator's undulator are tuned at 32.4 nm and the dispersive section $R_{56} = 63$ μm. Black bold solid line shows the averaged spectrum over 10 shots (rms bandwidth: 3.3×10^{-3}).

suppressed, i.e., $\delta_{\lambda_r} = \delta_{\mathrm{FEL}}$. The possibility to operate a HGHG FEL in SASE mode with the optical klystron scheme offers a number of opportunities. Despite the different spectral and temporal properties, the SASE operation mode is a backup solution providing an energy per pulse similar to that available in seeded mode, when the seed laser is unavailable. In addition users can benefit by the possibility of having alternatively the FEL in seeded and SASE optical klystron mode, to investigate particular phenomena depending on the longitudinal coherence. Finally, the optical klystron concept may be included in the design of future SASE FEL facilities leading to a significant reduction of the undulator length, or in existing FELs, where this scheme would allow reaching saturation earlier along the undulator, leaving room for efficiency enhancement via tapering of the rest of the undulator.

Authors are grateful to all the FERMI commissioning team for the valuable support in the optimization of the machine during the described experiments and the PADReS team for the help in delivering the radiation to the end-station.

*giuseppe.penco@elettra.eu

[1] A. L. Schawlow and C. H. Townes, Phys. Rev. **112**, 1940 (1958).
[2] T. H. Maiman, Nature (London) **187**, 493 (1960).
[3] W. Ackermann *et al.*, Nat. Photonics **1**, 336 (2007).
[4] E. Allaria *et al.*, Nat. Photonics **6**, 699 (2012).
[5] E. Allaria *et al.*, Nat. Photonics **7**, 913 (2013).
[6] P. Emma *et al.*, Nat. Photonics **4**, 641 (2010).
[7] T. Ishikawa *et al.*, Nat. Photonics **6**, 540 (2012).
[8] J. M. J. Madey, Phys. Rev. ST Accel. Beams **17**, 074901 (2014).
[9] G. Neil, J. Infrared, Millimeter, Terahertz Waves **35**, 5 (2014).
[10] G. Gallerano, A. Doria, E. Giovenale, and I. Spassovsky, J. Infrared, Millimeter, Terahertz Waves **35**, 17 (2014).
[11] A. S. Artamonov, N. A. Vinokurov, P. D. Voblyi, E. S. Gluskin, G. A. Kornyukhin, V. A. Kochubei, G. N. Kulipanov, V. N. Litvinenko, N. A. Mezentsev, and A. N. Skrinsky, Nucl. Instrum. Methods **177**, 247 (1980).
[12] G. A. Kornyukhin, G. N. Kulipanov, V. N. Litvinenko, N. A. Mesentsev, A. N. Skrinsky, N. A. Vinokurov, and P. D. Voblyi, Nucl. Instrum. Methods Phys. Res., Sect. A **237**, 281 (1985).
[13] M. Billardon, P. Elleaume, J. Ortega, C. Bazin, M. Bergher, M. Velghe, Y. Petroff, D. Deacon, K. Robinson, and J. Madey, Phys. Rev. Lett. **51**, 1652 (1983).
[14] M. Billardon, P. Elleaume, J. M. Ortega, C. Bazin, M. Bergher, M. E. Couprie, Y. Lapierre, R. Prazeres, M. Velghe, and Y. Petroff, Europhys. Lett. **3**, 689 (1987).
[15] R. Walker *et al.*, Nucl. Instrum. Methods Phys. Res., Sect. A **475**, 20 (2001).
[16] G. De Ninno *et al.*, Phys. Rev. Lett. **100**, 104801 (2008).
[17] V. N. Litvinenko, S. Hee Park, I. V. Pinayev, and Y. Wu, Nucl. Instrum. Methods Phys. Res., Sect. A **475**, 195 (2001).
[18] Y. K. Wu, N. A. Vinokurov, S. Mikhailov, J. Li, and V. Popov, Phys. Rev. Lett. **96**, 224801 (2006).
[19] N. A. Vinokurov and A. N. Skrinsky, Budker Institute for Nuclear Physics Report No. BINP 77–59, 1977.
[20] P. Ellaume, J. Phys. Colloques **44**, 333 (1983).
[21] H. Haus, IEEE J. Quantum Electron. **17**, 1427 (1981).
[22] G. Dattoli, A. Marino, A. Renieri, and F. Romanelli, IEEE J. Quantum Electron. **17**, 1371 (1981).
[23] R. Bonifacio, C. Pellegrini, and L. Narducci, Opt. Commun. **50**, 373 (1984).
[24] R. Bonifacio *et al.*, Riv. Nuovo Cimento **13**, 9 (1990).
[25] N. A. Vinokurov *et al.*, Nucl. Instrum. Methods Phys. Res., Sect. A **375**, 264 (1996).
[26] S. J. Hahn and K. H. Pae, J. Korean Phys. Soc. **31**, 856 (1997).
[27] K. J. Kim, Nucl. Instrum. Methods Phys. Res., Sect. A **407**, 126 (1998).
[28] E. L. Saldin, E. A. Schneidmiller, and M. V. Yurkov, arXiv:physics/0308060v1.
[29] Y. Ding, P. Emma, Z. Huang, and V. Kumar, Phys. Rev. ST Accel. Beams **9**, 070702 (2006).
[30] L. H. Yu, Phys. Rev. A **44**, 5178 (1991).
[31] E. Allaria, C. Callegari, D. Cocco, W. M. Fawley, M. Kiskinova, C. Masciovecchio, and F. Parmigiani, New J. Phys. **12**, 075002 (2010)
[32] G. Penco *et al.*, JINST **8**, P05015 (2013).
[33] S. Di Mitri *et al.*, Nucl. Instrum. Methods Phys. Res., Sect. A, **608**, 19 (2009).
[34] S. Heifets, G. Stupakov, and S. Krinsky, Phys. Rev. ST Accel. Beams **5**, 064401 (2002).
[35] E. L. Saldin, E. A. Schneidmiller, and M. V. Yurkov, Nucl. Instrum. Methods Phys. Res., Sect. A **528**, 355 (2004).
[36] Z. Huang, M. Borland, P. Emma, J. Wu, C. Limborg, G. Stupakov, and J. Welch, Phys. Rev. ST Accel. Beams **7**, 074401 (2004).
[37] S. Spampinati *et al.*, in *Proceedings of the 2013 FEL Conference*, edited by C. Scholl and V. R. W. Schaa (Jacow, New York, 2013), p. WEPS067.
[38] S. Spampinati *et al.*, Phys. Rev. ST Accel. Beams (to be published).
[39] M. Zangrando *et al.*, in *Advances in X-ray Free-Electron Lasers: Radiation Schemes, X-ray Optics, and Instrumentation*, Vol. 8078 edited by T. Tschentscher and D. Cocco (SPIE, Prague, 2011), p. 80780I.
[40] C. J. Bocchetta *et al.*, http://www.elettra.trieste.it/FERMI.
[41] E. Saldin, E. Schneidmiller, and M. V. Yurkov, *The Physics of Free Electron Lasers* (Springer Science, New York, 2000).
[42] S. Reiche, Nucl. Instrum. Methods Phys. Res., Sect. A **429**, 243 (1999).